FERROELECTRICS

Control of polarization in bulk ferroelectrics by mechanical dislocation imprint

Marion Höfling[1], Xiandong Zhou[1], Lukas M. Riemer[2], Enrico Bruder[1], Binzhi Liu[3], Lin Zhou[3,4], Pedro B. Groszewicz†, Fangping Zhuo[1], Bai-Xiang Xu[1], Karsten Durst[1], Xiaoli Tan[3], Dragan Damjanovic[2], Jurij Koruza[1]*, Jürgen Rödel[1]*

Defects are essential to engineering the properties of functional materials ranging from semiconductors and superconductors to ferroics. Whereas point defects have been widely exploited, dislocations are commonly viewed as problematic for functional materials and not as a microstructural tool. We developed a method for mechanically imprinting dislocation networks that favorably skew the domain structure in bulk ferroelectrics and thereby tame the large switching polarization and make it available for functional harvesting. The resulting microstructure yields a strong mechanical restoring force to revert electric field–induced domain wall displacement on the macroscopic level and high pinning force on the local level. This induces a giant increase of the dielectric and electromechanical response at intermediate electric fields in barium titanate [electric field–dependent permittivity (ε_{33}) ≈ 5800 and large-signal piezoelectric coefficient (d_{33}*) ≈ 1890 picometers/volt]. Dislocation-based anisotropy delivers a different suite of tools with which to tailor functional materials.

Ferroelectricity, like ferromagnetism and superconductivity, belongs to the class of cooperative phenomena. Strain engineering allows us to substantially modify related properties of thin films with a judicious choice of substrate materials. Strain engineering has been demonstrated for ferromagnetic materials (*1*) and superconductors (*2*). For ferroelectric films, phase transition temperatures have been enhanced by 400°C (*3*), and even non-ferroelectric materials have been made ferroelectric (*4*). Introducing dislocations allows localized strain engineering and affects the polarization reversal process (*5*). Although dislocations are generally the cause of degraded performance in functional oxides and are usually avoided at all costs, there are some excellent examples demonstrating their utility. Dislocations enable strong vortex pinning in high-temperature superconductors (*6*) required for high critical currents, whereas in thermoelectrics, they increase the heat-to-electricity conversion efficiency by affecting phonon scattering (*7*). In oxides, dislocations are not only associated with the surrounding strain fields, but often also exhibit charged cores and screening space-charge layers (*8*). These peculiar mechanical and electrical characteristics offer a large, yet mostly unexplored, potential to alter not only thermal (*7*), but also electrical conductivity (*8*, *9*). Numerical simulations have also confirmed the potential for interaction of dislocations with fundamental order parameters such as spontaneous polarization (P_s) and strain (*10*, *11*).

Obtaining high intrinsic electromechanical response and manipulating the mobility of ferroelectric domain walls [labeled as extrinsic contribution (*12*)] are two key challenges that exist in bulk ferroelectrics. Some common approaches for increasing the ferroelectric properties are strain engineering (*4*), polarization rotation (*13*), construction of phase boundaries (*14*), and exploitation of critical points (*15*). State-of-the-art concepts to control domain wall motion include point defect doping (*16*, *17*), domain engineering (*18*, *19*), and texturing (*20*).

We developed a method that uses dislocations to interact with the fundamental order and field parameters of bulk ferroelectric oxides, i.e., polarization and strain, at different length scales. This directly affects the force on, and thereby the movement of, domain walls. It introduces a temperature-stable macroscopic restoring force acting against the applied electric field and allows us to tune the dielectric and electromechanical properties. We

[1]Department of Materials and Earth Sciences, Technical University of Darmstadt, 64287 Darmstadt, Germany. [2]Group for Ferroelectrics and Functional Oxides, École Polytechnique Fédérale de Lausanne, 1015 Lausanne, Switzerland. [3]Department of Materials Science and Engineering, Iowa State University, Ames, IA 50011, USA. [4]Ames Laboratory, U.S. Department of Energy, Ames, IA 50011, USA. †Present address: Department of Radiation Science and Technology, Delft University of Technology, Delft 2629JB, Netherlands. *Corresponding author. Email: koruza@ceramics.tu-darmstadt.de (J.K.); roedel@ceramics.tu-darmstadt.de (J.R.)

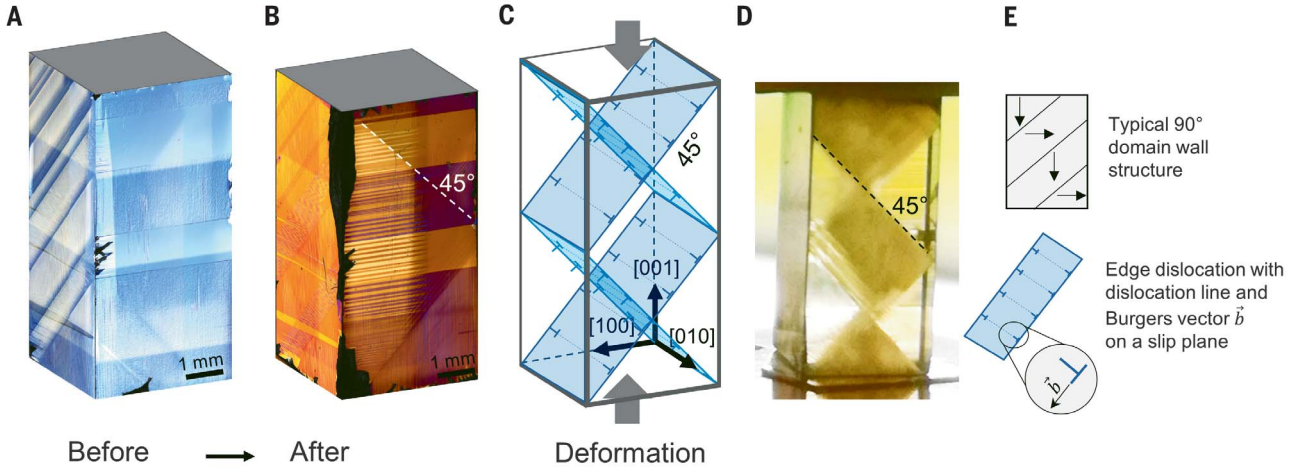

Fig. 1. Changes of the ferroelectric domain configuration by mechanical dislocation imprint. (**A**) Typical domain arrangement for a tetragonal <001>-oriented undeformed $BaTiO_3$ single crystal (*23*) imaged with differential interference contrast, which causes the change in color. (**B**) The same imaging method used for the deformed sample. (**C** and **D**) Schematic presentation of the set of slip systems {101}<101> activated during uniaxial deformation at high temperature. This introduces a directional dislocation network, resulting in a reorientation of the domains according to the slip planes highlighted in the diagram in (C), yielding a highly unusual rhombic domain structure in the photograph shown in (D). Both the cloudy and clear regions in (B) and (D) exhibit a multidomain state with different domain density (fig. S2). (**E**) Schematic of the typical 90° domain wall alignment and the dislocations with dislocation line and Burgers vector.

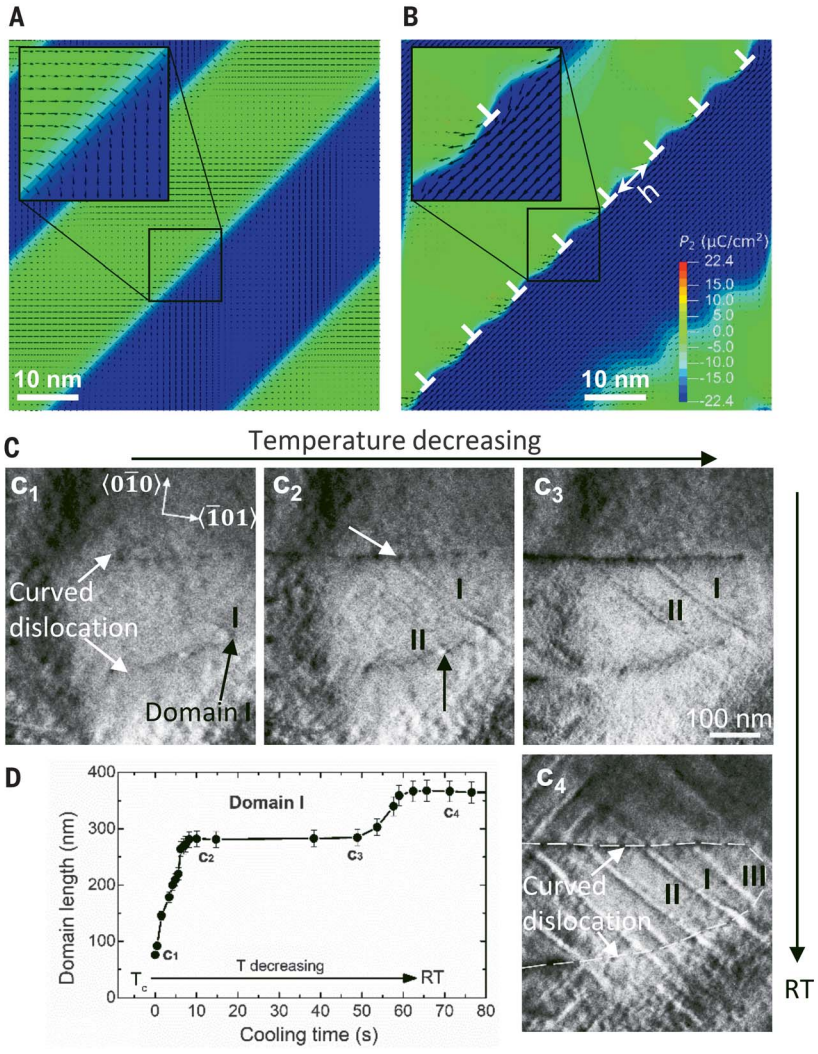

Fig. 2. Influence of dislocations on domain nucleation and mobility. (**A** and **B**) The steady state of local polarization without (A) and with (B) eight edge dislocations along the {101} plane as shown by phase-field simulations. Dislocations lead to both wavy domain walls and fluctuation of polarization amplitude, as demonstrated by the inset of (B). (**C**) In situ TEM study on a curved dislocation line during cooling through T_c (see movie S1). (**D**) Domain I nucleates at the lower segment of the dislocation (dark arrow in c_1), grows until it reaches the upper dislocation segment (white arrow in c_2), and is pinned there for a period of 40 s. Domains II (black arrow in c_2) and III are formed at the lower dislocation segment and grow until room temperature is reached (c_4). The temperature decrease is indicated with black arrows along the TEM images. Also shown is the link between simulated domain nucleation at the dislocation (B) and the formation of domains at the dislocation in temperature-dependent in situ TEM.

call our process mechanical dislocation imprinting because it is reminiscent of the mechanical imprinting used for engraving names or security codes. We also distinguish our process from one in which an electric charge is imprinted (*21*, *22*).

We used mechanical creep to introduce a directional dislocation network into <001>-oriented $BaTiO_3$ single crystals (fig. S1), and demonstrated that the dislocations act as nucleation sites for ferroelectric domain walls. The mechanical dislocation imprint causes a 19-fold increase in the large-signal piezoelectric coefficient (d_{33}*). Our methodology is readily accessible for furnishing bulk functional materials with permanent, tailored anisotropy.

The mechanical imprint is macroscopically reflected in the altered domain structure. The original lamellar domain configuration (*23*) (Fig. 1A) was changed into an unconventional rhombic domain structure with both clear and cloudy regions after high-temperature deformation (Fig. 1, B to D). Both regions exhibited a multidomain state with different domain density (fig. S2). The plastic deformation enforced an anisotropy with two-thirds of the domains in the deformed sample aligned along the deformation axis [001] (fig. S3). We used electron channeling contrast imaging (ECCI; fig. S4) to provide a microscopic view, featuring the orientation of imprinted glide planes on the surface. The dislocation spacing was in the range of 80 to 450 nm (fig. S4C). We used controlled indentation (fig. S4D) as a benchmark for the observed dislocation structures. We used transmission electron microscopy (TEM; fig. S5) to reveal a Burgers vector of $\boldsymbol{b} = a[101]$, where a is the lattice parameter. ECCI and TEM images confirmed the successful dislocation imprint by activation of the {101}<101> slip system.

Dislocations are associated with high local tensile and compressive stress fields (fig. S6, A and B) and, in some oxides, with a charged dislocation core. In ferroelectrics, this prompts a nucleation of domain walls (*24*). In our samples, this resulted in a rhombic domain structure (Fig. 1, B and D). We investigated the influence of the dislocations on the domain structure and the switching behavior using mechanically coupled phase-field (PF) simulations based on Ginzburg-Landau equations. The P_2 polarization component for a stable equilibrium configuration without dislocations is depicted in Fig. 2A, whereby straight 90° domain walls were formed on the {101} plane. We simulated the active slip system (Fig. 2B) with eight edge dislocations (Burgers vector $|\boldsymbol{b}| = 0.56$ nm), forming a dislocation array with $\boldsymbol{b} = a[101]$. From these results, we determined that the domain wall becomes kinked and broadens in the vicinity of a dislocation. Fluctuations of the local polarization and stress were strongly increased (Fig. 2B and fig. S6, A and B). This increase is in agreement with previous simulations investigating the impact of dislocation spacing, h, Burgers vector, and the strength of the dislocation-domain domain wall interaction (*10*, *11*) on the fluctuation of the local polarization.

We found a domain wall pinning effect of the dislocations using temperature-dependent in situ TEM, resulting in a controlled and localized nucleation and motion of the domain walls (Fig. 2C and movie S1). A similar effect had been predicted by simulations (*25*) and was reported in $Pb(Zr,Ti)O_3$ thin films with field-dependent in situ TEM (*26*). Upon cooling through the Curie temperature (T_c, 120°C), the first domain nucleated at the lower dislocation segment (I, dark arrow in Fig. 2C, c_1) and grew until it reached the upper dislocation segment. The latter pinned the domain temporarily (Fig. 2D) before it could overcome the dislocation barrier upon further cooling (Fig. 2C, c_4). At the same time, two new domains (II, III) nucleated at the lower dislocation segment. At room temperature (Fig. 2C, c_4), domain I was blocked by a {101} domain wall, whereas domains II and III were

still blocked by the upper dislocation segment. The dislocation-domain wall interactions that we observed in the TEM were corroborated by PF simulations as being a function of electric field and temperature (fig. S7, A and B).

Macroscopically, the increase in population density of *c*-domains (out-of-plane P_s) versus *a*-domains (in-plane P_s) in the unpoled sample (fig. S3) caused reduction of the permittivity after deformation (fig. S8A) due to anisotropy of the dielectric tensor of BT with $\varepsilon_a > \varepsilon_c$. By contrast, the poled deformed samples retained a high fraction of *a*-domains (fig. S3), leading to an enhanced permittivity (by a factor of five) compared with the reference samples. Clearly, domain wall density will also come into play (*18*), but this appears to be a secondary issue.

Application of large-signal super-coercive fields (Fig. 3A) highlights the substantial impact of mechanical dislocation imprint. Despite loop saturation, polarization did not reach the expected spontaneous polarization value of 26 μC/cm^2, indicating domain wall pinning. Concurrently, we observed a four-fold increase in domain back-switching ($P_{back} = P_{max}^* - P_{rem}^*$) compared with the undeformed reference samples (fig. S9), which indicates a strong macroscopic restoring force. The apparent coercive field (E_c^*), was strongly enhanced, supporting domain wall pinning (for statistical confirmation, see fig. S9).

The full potential of the dislocation-domain wall interaction was obtained in the intermediate E-field regime (below E_c^*). Increasing the amplitude of the applied AC electric field beyond the small-signal excitation resulted in stronger domain wall vibration, whereas the restoring force imposed by the presence of *a*-domains tuned this displacement and ensured a back-switching of domains in regions with high dislocation density. As a result, both the large-signal dielectric permittivity and the piezoelectric coefficient increased exponentially at ~E/E_c^* = 0.1 and reached $\varepsilon_{33}' \approx 5810$ and $d_{33}^* \approx 1890$ pm/V at E/E_c^* =0.17, respectively (Fig. 3B). The d_{33}^* value was ~19 times higher compared with the undeformed reference sample ($d_{33}^* \approx 98$ pm/V, $\varepsilon_{33}' \approx 170$). Because of the long-range restoring force, this domain wall motion was almost anhysteretic below E_c^* (fig. S10). Note that the high permittivity and piezoelectric coefficient values remained stable up to 130,000 AC cycles (fig. S11) and a temperature of 75°C (fig. S12, A and B). In addition, the overall behavior featured a weak frequency dependence in d_{33}^* (fig. S13).

Our results indicate that the uniaxial stress activated four out of six available glide planes. The ensuing dislocation networks stabilized two domain wall variants (a_1-*c* and a_2-*c*) but disfavored the a_1-a_2 variant (fig. S3). Therefore, the imprinted mechanical dislocation structure caused an anisotropy in the domain

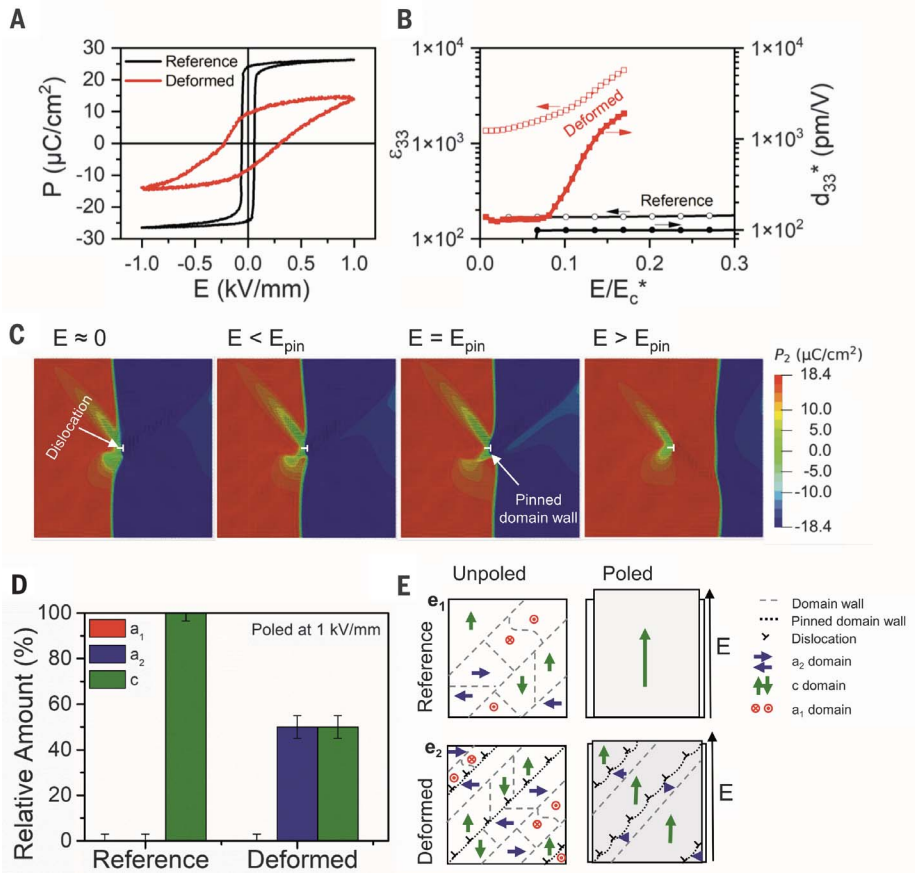

Fig. 3. Influence of mechanical dislocation imprint on electrical properties. (**A**) The presence of dislocations yields a decrease in P_{max}^* and pronounced back-switching. (**B**) Substantial increase in d_{33}^* and electric field–dependent permittivity (ε_{33}) for the poled deformed sample with increasing AC electric field (normalized by E_c^* at 1 kV/mm). (**C**) Simulation of the dislocation-domain wall interaction. When the electric field is relatively low, the domain wall is pinned at the dislocation and gets kinked and bent. When a pinning electric field is reached, the wall can break through the barrier of a single dislocation. (**D**) Comparison of the domain distribution of a reference and a deformed sample poled at 1 kV/mm, as obtained from nuclear magnetic resonance (NMR) measurements (fig. S3). (**E**) Schematic depiction of the domain structures. Due to pinning of the *a*-*c* domain walls at the dislocation and the resulting macroscopic restoring force, the total net expansion in the *c* direction is reduced compared with the undeformed reference sample, but the switchable strain is strongly enhanced.

structure, both in the unpoled and the poled state. The enforced presence of the *a*-domains provided a strain incompatibility to electric field–enforced *c*-domains, resulting in an elastic macroscopic restoring force akin to the case of thin films, in which the strain incompatibility is provided by the substrate. Locally, the dislocation network sitting on exactly the same plane as the domain wall provided a pinning force. The latter was confirmed by our numerical model (Fig. 3C) demonstrating pinning of a domain wall at a single dislocation. Domain wall bending and reversible domain wall movement increased up to $E = E_{pin}$ [pinning electric field]. Above E_{pin}, the domain wall overcame the local pinning potential. At the pinning electric field, domain walls at glide planes with low dislocation density became locally unpinned in an irreversible manner, but the overall remaining strain incompatibility ensured by glide planes with high dislocation density stabilized the *a*-*c* domain wall variant (Fig. 3D and fig. S14) and ensured complete back-switching (fig. S15). We visualized the increased density of *a*-*c* domain walls after deformation in the unpoled and poled state (Fig. 3E). We observed that mechanical dislocation imprint maintained a thermally stable piezoelectric coefficient up to 75°C. In a $SrTiO_3$ perovskite, dislocation structures have been reported to feature stability up to 600°C (*8*), offering pinning sites in a large temperature range. Similar reversal to the domain structure at zero electric field can only be enforced by external mechanical compressive stress (*27*). Current material design options include the use of point defects (*17*) or complex poling conditions stabilizing independently

a-domains and *c*-domains in different sample volumes (*19*). These design options until now have not been used for practical purposes because they are stable only for a limited number of electrical cycles and at low temperatures (*19*) or limited electric field levels (*20*). Our dislocation-based mechanism is fundamentally different from acceptor doping (*17*), in which pinning centers are homogeneously distributed, allowing only relatively short motion of domain walls. In mechanically deformed samples, dislocations are concentrated in some parts of the sample and depinned domain walls can therefore move for longer distances. In bulk ceramics, templated grain growth (*28*, *29*) affords outstanding properties, as demonstrated for energy storage materials with supreme reliability (*30*).

Mechanical dislocation imprinting provides a powerful mechanism to extend the local pinning potential of dislocations to the macroscopic level of bulk ceramics. Whereas in thin films, the substrate provides the tool for strain engineering and misfit dislocations are indispensable (*31*), in bulk materials, dislocations have to be introduced through creep, plastic deformation, or new methods such as flash sintering (*32*). Uniaxial stress selects a specific dislocation structure that installs the in-plane strain permanently into the volume, thus providing a macroscopic restoring force. In addition, this method provides a dislocation structure for local effects such as domain wall pinning. This mechanical dislocation imprint both tames strong domain wall switching under applied electric field and allows the harvesting of this strain change caused by mechanically enforced back-switching. Subcoercive electric fields therefore reach extraordinary piezoelectric coefficients. This mechanism extends the available spectrum of tools for designing the functional properties of bulk functional materials such as ferroics and superconductors.

REFERENCES AND NOTES

1. R. S. Beach *et al.*, *Phys. Rev. Lett.* **70**, 3502–3505 (1993).
2. I. Bozovic, G. Logvenov, I. Belca, B. Narimbetov, I. Sveklo, *Phys. Rev. Lett.* **89**, 107001 (2002).
3. K. J. Choi *et al.*, *Science* **306**, 1005–1009 (2004).
4. J. H. Haeni *et al.*, *Nature* **430**, 758–761 (2004).
5. S. V. Kalinin *et al.*, *Adv. Mater.* **22**, 314–322 (2010).
6. B. Dam *et al.*, *Nature* **399**, 439–442 (1999).
7. S. I. Kim *et al.*, *Science* **348**, 109–114 (2015).
8. K. K. Adepalli, J. Yang, J. Maier, H. L. Tuller, B. Yildiz, *Adv. Funct. Mater.* **27**, 1700243–1700249 (2017).
9. L. Porz *et al.*, *ACS Nano* acsnano.0c04491 (2020).
10. A. Kontsos, C. M. Landis, *Int. J. Solids Struct.* **46**, 1491–1498 (2009).
11. H. H. Wu, J. Wang, S. G. Cao, T. Y. Zhang, *Appl. Phys. Lett.* **102**, 232904 (2013).
12. D. Damjanovic, *Rep. Prog. Phys.* **61**, 1267–1324 (1998).
13. H. Fu, R. E. Cohen, *Nature* **403**, 281–283 (2000).
14. R. Guo *et al.*, *Phys. Rev. Lett.* **84**, 5423–5426 (2000).
15. Z. Kutnjak, J. Petzelt, R. Blinc, *Nature* **441**, 956–959 (2006).
16. K. Carl, K. H. Härdtl, *Ferroelectrics* **17**, 473–486 (1978).
17. X. Ren, *Nat. Mater.* **3**, 91–94 (2004).
18. S. Wada *et al.*, *Ferroelectrics* **355**, 37–49 (2007).
19. Q. Wang, F. Li, *J. Phys. D Appl. Phys.* **51**, 255301 (2018).
20. Y. Saito *et al.*, *Nature* **432**, 84–87 (2004).
21. N. Hur *et al.*, *Nature* **429**, 392–395 (2004).
22. B. Akkopru-Akgun, W. Zhu, M. T. Lanagan, S. Trolier-McKinstry, *J. Am. Ceram. Soc.* **102**, 5328–5341 (2019).
23. W. J. Merz, *Phys. Rev.* **88**, 421–422 (1952).
24. R. C. Bradt, G. S. Ansell, *J. Appl. Phys.* **38**, 5407–5408 (1967).
25. S. Y. Hu, Y. L. Li, L. Q. Chen, *J. Appl. Phys.* **94**, 2542–2547 (2003).
26. P. Gao *et al.*, *Nat. Commun.* **2**, 591 (2011).
27. E. Burcsu, G. Ravichandran, K. Bhattacharya, *Appl. Phys. Lett.* **77**, 1698–1700 (2000).
28. G. L. Messing *et al.*, *J. Mater. Res.* **32**, 3219–3241 (2017).
29. S. Kong, J. Daniels, *Appl. Phys. Lett.* **117**, 182901 (2020).
30. J. Li *et al.*, *Nat. Mater.* **19**, 999–1005 (2020).
31. M. W. Chu *et al.*, *Nat. Mater.* **3**, 87–90 (2004).
32. J. Cho *et al.*, *Mater. Res. Lett.* **7**, 194–202 (2019).

ACKNOWLEDGMENTS

We thank S. Bauer and K. Ding for providing the reference indent in $BaTiO_3$, J. Lins for the acquisition of the NMR spectra, and G. Buntkowsky for access to the NMR spectrometer. B.X-X. and X.Z. thank the HHLR, Technical University of Darmstadt, for access to the Lichtenberg High-Performance Computer and for technical support. **Funding:** This work is supported by project no. 414179371 of the German Research Foundation (DFG). The TEM experiments, performed at the Sensitive Instrument Facility at Ames Laboratory, were supported by the U.S. National Science Foundation (NSF) through grant no. DMR-1700014. J.K. acknowledges financial support from the Athene Young Investigator program of TU Darmstadt. L.M.R. acknowledges financial support from the Swiss National Science Foundation (grant no. 200021 172525). P.B.G. and J.K. acknowledge the Profile Area "PMP" of TU Darmstadt for providing the goniometer NMR probe. The PF simulation work was partially funded by project no. 398072825 of DFG. **Author contributions:** M.H. prepared the samples. M.H. and L.M.R. performed the dielectric and electromechanical measurements. F.Z. provided confirmation on an independent orientation. J.R. and J.K. designed the experiments and, together with D.D., supervised the analysis of the data. X.Z. and B.X-X. performed the phase field simulations. B.L., L.Z., and X.T. performed the TEM analysis. P.B.G. planned and analyzed the NMR measurements and E.B. the ECCI measurements. D.D., J.R., J.K., M.H., and K.D. discussed the deformation mechanisms. M.H., J.K., and J.R. prepared the manuscript. All authors contributed and commented on the text. **Competing interests:** The authors declare no competing interests. **Data and materials availability:** All data are available in the main text or the supplementary materials.

SUPPLEMENTARY MATERIALS

science.sciencemag.org/content/372/6545/961/suppl/DC1
Materials and Methods
Supplementary Text
Figs. S1 to S15
Movie S1
References (*33*–*50*)

18 August 2020; accepted 26 April 2021
10.1126/science.abe3810

Science

Control of polarization in bulk ferroelectrics by mechanical dislocation imprint

Marion Höfling, Xiandong Zhou, Lukas M. Riemer, Enrico Bruder, Binzhi Liu, Lin Zhou, Pedro B. Groszewicz, Fangping Zhuo, Bai-Xiang Xu, Karsten Durst, Xiaoli Tan, Dragan Damjanovic, Jurij Koruza and Jürgen Rödel

Science **372** (6545), 961-964.
DOI: 10.1126/science.abe3810

Imprinting oxides

Dislocations can be problematic for the properties of functional oxides and are often avoided as a result. Höfling *et al.* found that introducing a network of dislocations to barium titanate actually enhanced the dielectric and piezoelectric properties. The authors introduced the dislocation network with uniaxial compression, which forced the material to have a domain structure that enhanced the piezoelectric coefficient by a factor of 19. This strategy should be a useful tool for optimizing properties of other functional oxides.

Science, abe3810, this issue p. 961